Energy Proceedings
Vol 26, 2022
ISSN 2004-2965

Experimental and Numerical Investigation of the Effect of Geometric Parameters on the Charging and Discharging Performance of a Vertical Latent Heat Thermal Energy Storage Unit

Bohui Lu [1, 2], Yongxue Zhang[1, 2*]

1 College of Mechanical and Transportation Engineering, China University of Petroleum, Beijing 102249, China

2 Beijing Key Laboratory of Process Fluid Filtration and Separation, Beijing 102249, China

ABSTRACT

The latent heat thermal energy storage (LHTES) unit with shell and tube type is widely considered to be one of the most competitive technologies to store and use solar energy thanks to its high thermal storage density, low cost and little temperature fluctuation. The phase change material (PCM) is filled in the annular space between the inner shell and outer tube, while the heat transfer fluid (HTF) flowing through the inner tube. However, the heat transfer process during the melting and solidification processes of PCM is complicated involving heat conduction, natural convection and solid-liquid phase change, which is closely related to the geometric parameters of LHTES unit. Thus, the main purpose of the current study is to explore the effect of geometric parameters on the charging and discharging performances of the LHTES unit. Firstly, a visual experiment was carried out to observe the evolution of the solid-liquid interface and monitor the temperature variation of PCM during the melting and solidification processes. Then, a two-dimensional numerical model was established and validated by the experimental data to investigate the effect of geometric parameters on the charging and discharging performances. Four kinds of geometric parameters with different shell heights were designed and studied under the same volume and heat transfer area of PCM. Results demonstrated that during the melting process, the complete melting time increases with an increase of the shell height, vice versa for the solidification process. When the height of shell increases from 100 mm to 400 mm under the same HTF inlet temperature and flow rate, the complete melting time can be increased by 20.14% and the complete solidification time is saved by 22.87%. This means that the geometric parameters of LHTES unit should be designed carefully to comprehensively consider the weightings of the charging and discharging processes in practical applications.

Keywords: Latent heat thermal energy storage, Phase change material, Shell and tube, Charging and discharging performance, Geometric parameter

NONMENCLATURE

Abbreviations	
HTF	Heat transfer fuid
LHTES	Latent heat thermal energy storage
PCM	Phase change material
Symbols	
A_{mush}	Mush zone constant (-)
c_p	Specific heat capacity (kJ/(kg·K))
$\boldsymbol{g}$	Gravitational acceleration (m/s^2)
h	Sensible enthalpy (J/g)
H	Enthalpy (J/g)
h_c	Convective heat transfer coefficient (W/(m^2·K))
H_s	Height (mm)
k	Thermal conductivity (W/(m·K)
L	Latent heat (J/g)
p	Pressure (Pa)
q	Heat flux (W/m^2)
r	Tube radius (mm)
R	Shell radius (mm)
S	Area (mm^2)
T	Temperature (K)
t	Time (s)
T_l	Liquidus temperature (K)
T_s	Solidus temperature (K)
$\boldsymbol{u}$	Velocity vector (m/s)
V	Volume (mm^3)
ΔH	Latent enthalpy (J/g)
Greek letters	
β	Thermal expansion coefficient (1/K)
δ	Wall thickness (mm)
ε	A very small number (-)
λ	Liquid fraction (-)
μ	Dynamic viscosity (Pa·s)
ρ	Density (kg/m^3)

1. INTRODUCTION

With the fast growing of environmental hazards resulted from the excessive consumption of fossil fuels, the renewable energy with pollution-free has received widespread attention in recent years [1]. However, the renewable energy, such as solar and wind energy, suffers from discontinuity and imbalances of intensity, time and space, which are the main obstacle during the development and utilization of pollution-free energies [2]. Thus, the latent heat thermal energy storage (LHTES) technology adopting phase change material (PCM) has become a promising solution to solve this problem due to its high thermal storage density and mild temperature fluctuation [3, 4].

Unfortunately, the charging and discharging rates of LHTES unit are not sufficient for its industrial application because of the poor thermal conductivities of available PCMs [5]. For this reason, a large amount of research for enhancing the melting and solidification rate of PCM has been reported, such as installing the fins to increase the heat transfer area [6], adding nanomaterials to improve the thermal conductivity [7] and immersing them into the porous material to obtain the internal heat transfer path [8]. Besides, the melting and solidification rate of PCM can also be enhanced by diminishing the nonuniformity of phase change process caused by natural convection of liquid PCM [9]. On one hand, the phenomenon of natural convection is closely related to the geometric parameters of LHTES unit [10]. On the other hand, LHTES unit with shell and tube has become a research focal in industry and academia due to its low cost, simple structure and easy manufacturing [11]. Nevertheless, only few researchers have studied the geometrical effects on the charging and discharging performances of LHTES unit. Seddegh et al. [12] experimentally investigated the effect of radius ratio between shell and tube on the charging process of LHTES unit. It was found that the LHTES unit with radius ratio of 5.4 exhibited remarkable performance both in melting time and heat stored. Fornarelli et al. [13] numerically compared the melting phase change of LHTES unit with four different radius ratios. Their results demonstrated that the melting time can be reduced by 50% for radius ratio of 1.5 compared with that of 4.375. In addition, the volume and the heat transfer area of PCM are two important parameters for LHTES unit. The former one determines how much thermal energy can be stored, and the latter one determines how much heat transfer tube material is required. Hence, the optimization of geometric parameters of LHTES unit should be carried out with the same PCM volume and heat transfer area.

Currently, few studies are available in literature aiming at the reliable design standard for LHTES unit. The question of what the optimal configuration of parameters of LHTES unit is has not been well answered. The objective of this work is to investigate the effect of geometric parameters on the charging and discharging performances of LHTES unit when the volume and the heat exchange area of PCM maintain constant.

2. MATERIALS AND METHODS

2.1 Material

Paraffin with relatively high latent heat and narrow phase change range was selected as PCM, which was purchased from Zhongjia new material Co., Ltd, Guangzhou, China. All the thermo-physical properties of the paraffin were measured by in-house instrumentations in our study, which are summarized in Table 1 below. In the following research, the specific heat, thermal conductivity and viscosity are assumed to be in linear functions of temperature.

Table 1 Thermo-physical properties of paraffin

Property	Melting	Solidification
ρ (kg/m3)	826.24 (60℃)	826.24 (60℃)
T_s (K)	321.28	313.43
T_l (K)	329.78	321.69
L (J/g)	203.56	200.46
β (1/K)	0.001023	0.001023
c_p (J/(kg·K))	1797 (15℃)	1836 (15℃)
	2251 (65℃)	2140 (65℃)
k (W/(m·K))	0.2687(25℃)	0.2687 (25℃)
	0.1805 (65℃)	0.1805 (65℃)
μ (Pa·s)	0.007062 (60℃)	0.007062 (60℃)
	0.005323 (70℃)	0.005323 (70℃)

2.2 Experimental setup

An experimental setup was designed and established to investigate the melting and solidification behaviors of paraffin in a LHTES unit with vertical shell and tube and to validate the accuracy of numerical model, as shown in Fig. 1 (a). The acrylic-made shell geometries are 60 mm inner diameter, 5 mm thickness and 300 mm height. The inner diameter and thickness of middle-brass-made tube are taken as 14.7 mm and 2.9 mm, respectively. Apart from the main pipe, the entrance and exit of the LHTES unit, nine PT-100 thermo resistors are installed isometrically in the PCM zone, as can be seen in Fig. 2 (b).

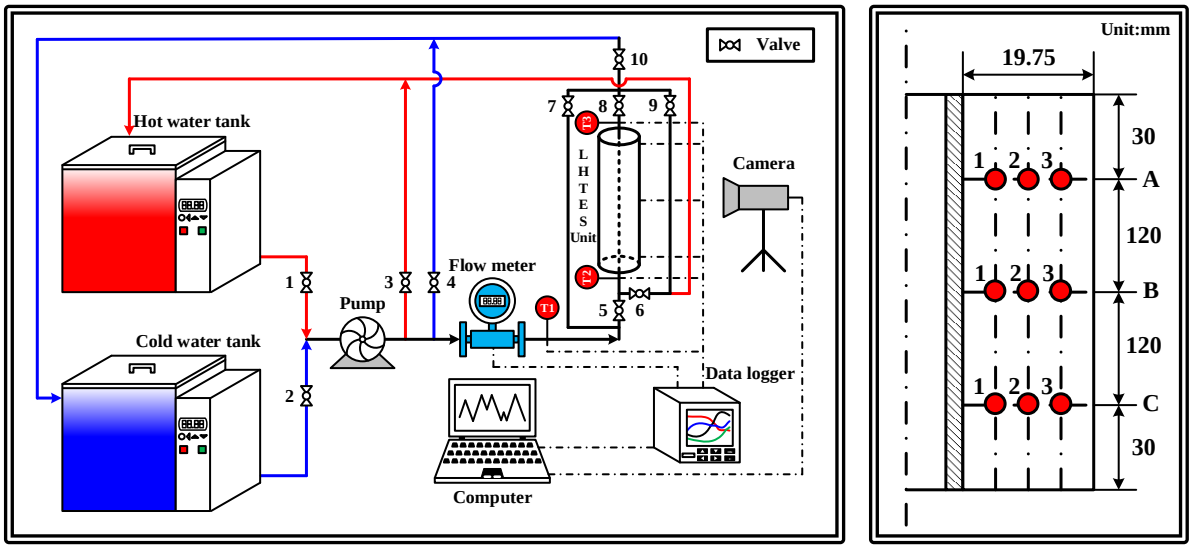

(a) *(b)*

Fig. 1 (a) Schematic diagram of experimental setup; (b) Locations of PT-100 thermo resistors

2.3 Numerical method

Fig. 2 (a) presents the physical model of LHTES unit during charging and discharging processes. It can be simplified to 2D computational model due to its axisymmetric structure to save computing resources and accelerate the computing efficiency, as shown in Fig. 2 (b).

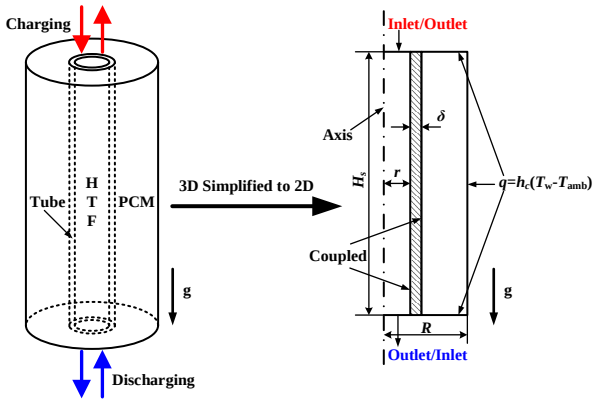

(a) *(b)*

Fig. 2 (a) Physical model and (b) simplified computational model of LHTES unit

This computational model is comprised of the domains of HTF, PCM and tube. The flow and heat transfer processes of these domains are governed as follows:

For the HTF

$$\nabla \cdot \boldsymbol{u} = 0 \tag{1}$$

$$\rho_{\mathrm{HTF}} \frac{\partial \boldsymbol{u}}{\partial t} + \rho_{\mathrm{HTF}} \left(\boldsymbol{u} \cdot \nabla\right)\boldsymbol{u} = -\nabla p + \mu_{\mathrm{HTF}} \nabla^2 \boldsymbol{u} + \rho_{\mathrm{HTF}} \boldsymbol{g} \tag{2}$$

$$\rho_{\mathrm{HTF}} c_{\mathrm{p,HTF}} \frac{\partial T}{\partial t} + \rho_{\mathrm{HTF}} c_{\mathrm{p,HTF}} \boldsymbol{u} \cdot \nabla T = \nabla \cdot \left(k_{\mathrm{HTF}} \nabla T\right) \tag{3}$$

For the PCM

$$\nabla \cdot \boldsymbol{u} = 0 \tag{4}$$

$$\rho_{\mathrm{PCM}} \frac{\partial \boldsymbol{u}}{\partial t} + \rho_{\mathrm{PCM}} \left(\boldsymbol{u} \cdot \nabla\right)\boldsymbol{u} = -\nabla p + \mu_{\mathrm{PCM}} \nabla^2 \boldsymbol{u} + \rho_{\mathrm{PCM}} \boldsymbol{g} \beta \left(T - T_{\mathrm{ref}}\right) - \frac{\left(1-\lambda\right)^2}{\lambda^3 + \varepsilon} A_{\mathrm{mush}} \boldsymbol{u} \tag{5}$$

$$\rho_{\mathrm{PCM}} \frac{\partial H}{\partial t} + \rho_{\mathrm{PCM}} \nabla \cdot \left(\boldsymbol{u} H\right) = \nabla \cdot \left(k_{\mathrm{PCM}} \nabla T\right) \tag{6}$$

Enthalpy (H) is obtained by the sum of sensible (h) and latent heat (ΔH):

$$H = h + \Delta H = h_{\mathrm{ref}} + \int_{T_{\mathrm{ref}}}^{T} c_{\mathrm{p,PCM}} dT + \lambda L \tag{7}$$

Liquid fraction (λ) is calculated by:

$$\lambda = \begin{cases} 0 & T < T_{\mathrm{s}} \\ \dfrac{T - T_{\mathrm{s}}}{T_{\mathrm{l}} - T_{\mathrm{s}}} & T_{\mathrm{s}} \le T \le T_{\mathrm{l}} \\ 1 & T_{\mathrm{l}} < T \end{cases} \tag{8}$$

For the tube

$$\rho_{\mathrm{tube}} c_{\mathrm{p,tube}} \frac{\partial T}{\partial t} = \nabla \cdot \left(k_{\mathrm{tube}} \nabla T\right) \tag{9}$$

where $\boldsymbol{u}$ is velocity vector, ρ is density, t is time, p is pressure, μ is dynamic viscosity, $\boldsymbol{g}$ is gravitational acceleration, c_p is specific heat capacity, T is temperature, k is thermal conductivity, β is volume thermal expansivity. $\varepsilon=10^{-3}$ to avoid denominator is zero, A_{mush} ranging from 10^5 to 10^7 [14] is mush zone constant and 10^7 is adopted in this study due to the good agreement with experimental data.

During the charging process, the initial temperatures of all domains were 20 ℃. HTF with the temperature of 80 ℃ and flow rate of 1 L/min was injected into LHTES unit from top to bottom. During the discharging process, the initial temperatures of all domains were 62 ℃. HTF with the temperature of 10 ℃ and flow rate of 1 L/min was injected into LHTES unit from bottom to top. The inner and outer walls of tube were coupled boundaries. The heat loss between LHTES unit and environment was considered by heat convection.

Three girds (node number of 2396, 5156 and 9296) and time steps (0.2 s, 0.5 s and 1.0 s) were used to check the grid and time step independence. It is found from Fig. 3 that the gird with node number of 5156 and the time step of 0.5 s is sufficient to ensure the numerical accuracy. Fig. 4 compares the temperature and liquid fraction versus time of experimental and simulated results during charging and discharging processes. It can be observed that these two methods show a good agreement.

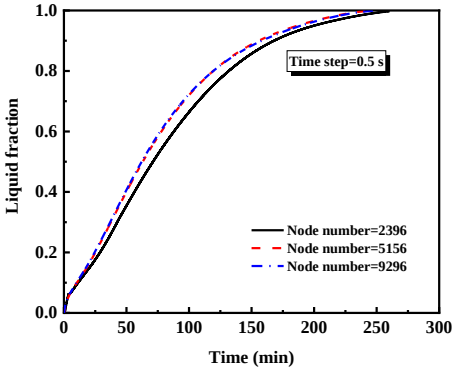

(a)

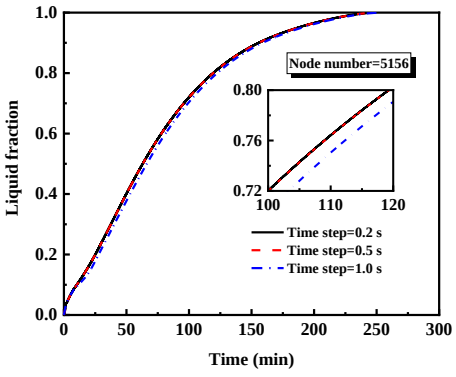

(b)

Fig. 3. Grid (a) and time (b) step independence test.

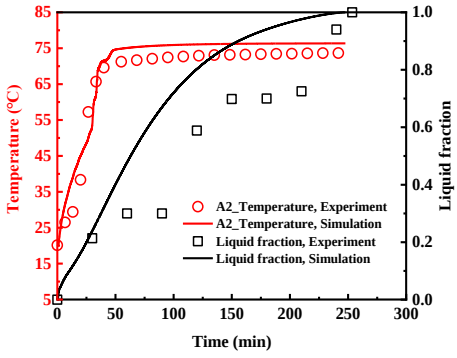

(a)

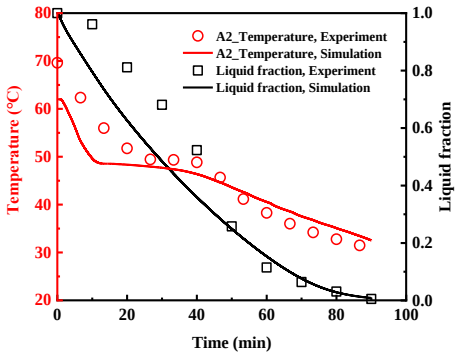

(b)

Fig. 4 Comparisons of temperature and liquid fraction versus time of experimental and simulated results during (a) charging and (b) discharging processes.

3. RESULTS AND DISCUSSION

3.1 Charging and discharging processes

The local temperature change of PCM, liquid fraction contours and pictures of PCM during the charging and discharging processes are presented in Fig. 5 and Fig. 6, respectively. At the beginning of the charging process, the temperature of level A increases rapidly as the liquid PCM flows upward driven by thermal buoyancy. By contrast, the rates of temperature increase of level B and level C are relative slow due to that the heat transfer is deaminated by heat conduction in the solid PCM. With the melting front evolution from top to bottom, the rate of temperature increase in level B is gradually accelerated until all of the PCM at this level becomes liquid state. It also can be seen that level C is located at the bottom of LHTES unit, and it takes the longest time to melt completely since the distance between level C and the melting front is relatively long and the heat conduction dominates within a long period. When the temperatures of all levels are higher than the liquid temperature of PCM, a dynamic thermal balance is reached inside the LHTES unit and the temperature of PCM will not rise sharply due to the existence of heat loss.

The initial temperature of PCM varies for different levels during the discharging process due to the effect of natural convection of liquid PCM. Unlike the charging

process, it can be observed that the rate of temperature decrease is very fast in the initial discharging process. This is because thermal energy is released in the form of sensible heat and a large temperature difference between PCM and HTF holds. Subsequently, the PCM temperature decline trend abruptly changes owing to the large latent heat of PCM. Interestingly, the temperature decrease rate of level A is higher than that of level B when the level A temperature is lower than the liquid temperature of PCM. Since the volume of PCM shrinks during solidification, less heat is required to solidify PCM around level A.

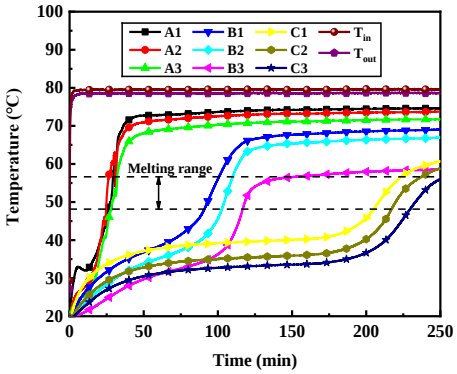

(a)

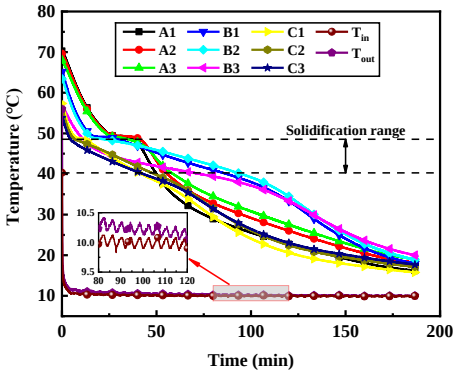

(b)

Fig. 5 Temperature change of local PCM during (a) charging and (b) discharging processes.

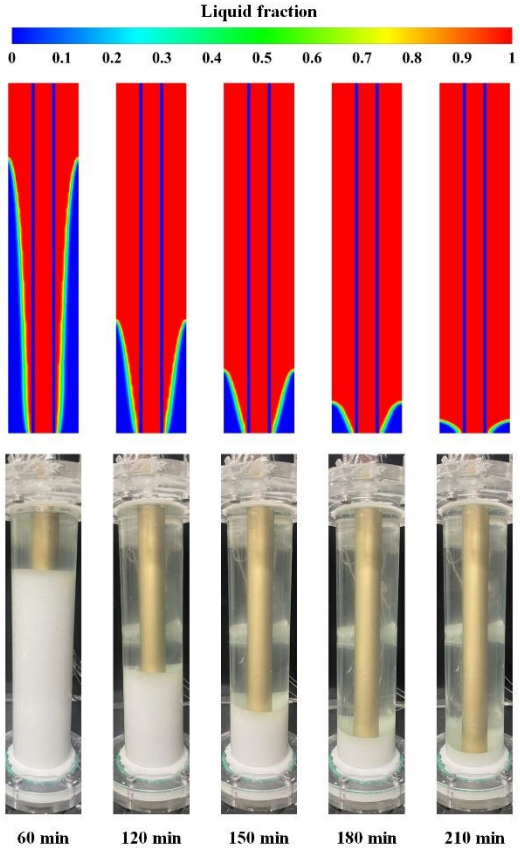

(a)

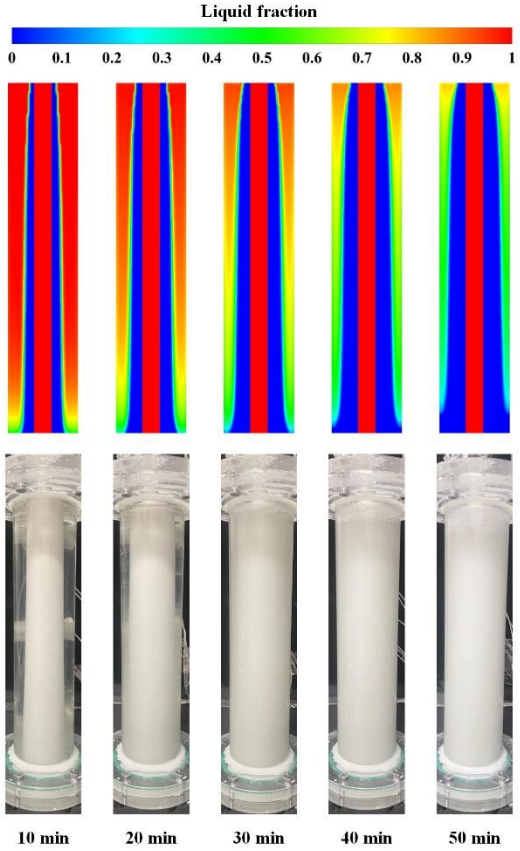

(b)

Fig. 6 Liquid fraction contours and pictures of PCM during (a) charging and (b) discharging processes

3.2 Effect of geometric parameters

To study the effect of geometric parameters of LHTE unit on the charging and discharging performances, the height was selected as the control variable since it is the only variable when the volume and heat transfer area of PCM keep constant. The geometric dimensions are listed in Table 2.

Table 2 The geometric dimensions of shell shape.

Cases	Hs (mm)	R(mm)	r(mm)	δ (mm)	V (mm^3)	S (mm^2)
Case Ⅰ	100	57.71	27.85	2.90	748831	19311
Case Ⅱ	200	37.80	12.48	2.90	748831	19311
Case Ⅲ	300	30.00	7.35	2.90	748831	19311
Case Ⅳ	400	25.60	4.79	2.90	748831	19311

Fig. 7 demonstrates the liquid fraction, melting/solidification time and heat stored/released for four cases during charging and discharging processes, and the liquid fraction contours are compared in Fig. 8. It can be seen from Fig. 7 (a) that the melting rate of PCM decreases with the increase of the height of LHTES unit at the final stage of the charging process. When the height increases from 100 mm to 400 mm, the melting time is increased by 20.14%, and the heat stored is increased by 1.2%. This is because that the motion of melting front of PCM is from top to bottom due to natural convection of melted PCM (see Fig. 8 (a)). The heat transfer distance increases with the increase of shell height, thereby leading to more time to complete melting for the solid PCM at the bottom region of higher height shell. As seen in Fig. 7 (b), the higher the height of LHTES unit, the faster the solidification rate of PCM. When the height increases from 100 mm to 400 mm, the solidification time is saved by 22.87%, and the heat released is increased by 2.68 %. This can be explained by the fact that the motion of solidification front of PCM is from inside to outside along the radius (see Fig. 8 (b)). The thermal resistance decreases as the radius shortens due to height increase, thus resulting in a faster solidification rate for higher height shell.

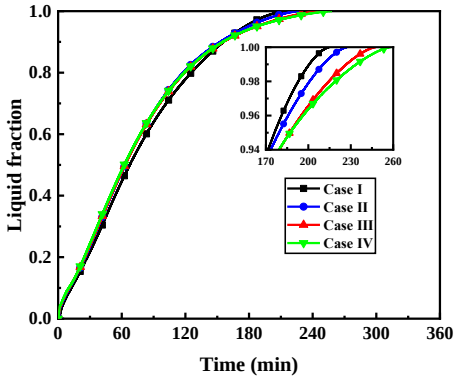

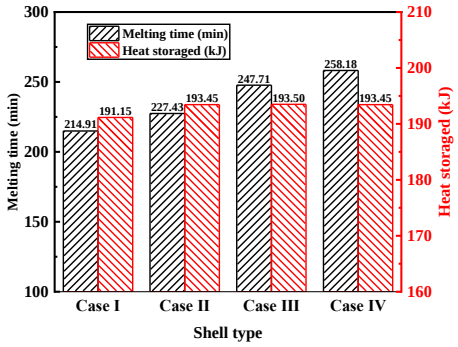

(a)

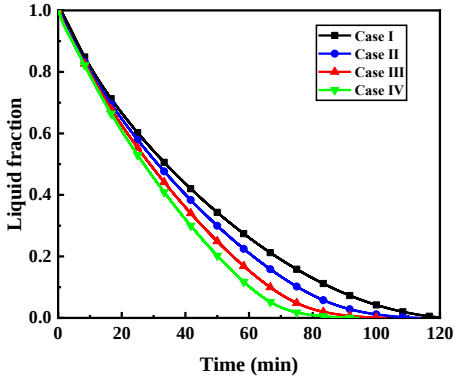

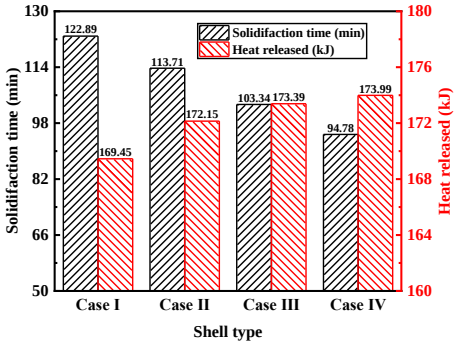

(b)

Fig. 7 Evolution of liquid fraction, melting/solidification time and heat stored/released for four cases during (a) charging and (b) discharging processes.

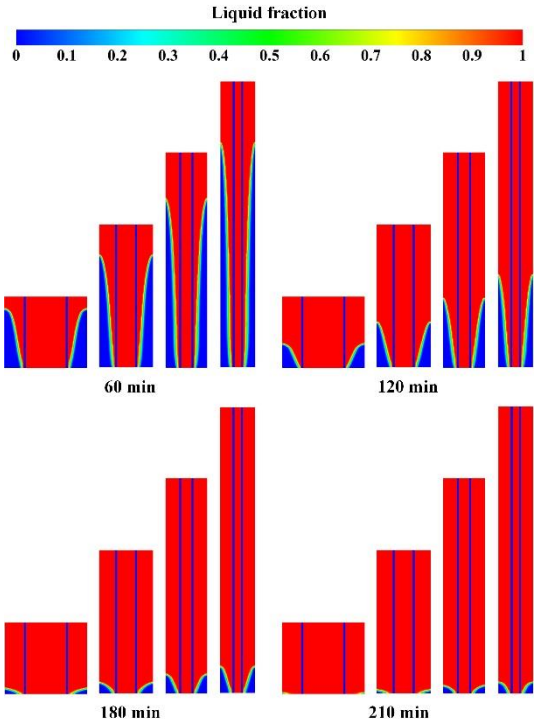

(a)

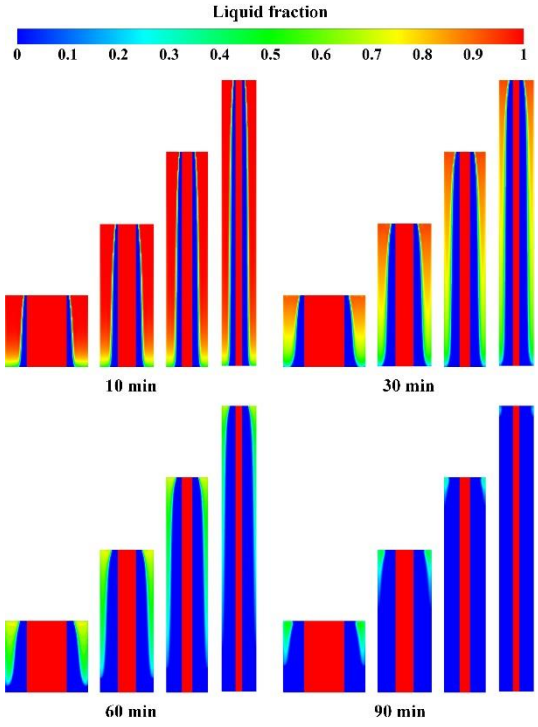

(b)

Fig. 8 Liquid fraction contours for four cases during (a) charging and (b) discharging processes.

4. CONCLUSIONS

Some conclusions can be derived from the research:

(1) The axial temperature differences of PCM are considerable due to the natural convection during the charging process, while it is relatively small for the discharging process.

(2) The LHTES unit with lager height can store and release more thermal energy compared to that with a smaller height.

(3) As the height of LHTES increases from 100 mm to 400 mm, the complete melting time increases by 20.14% and the complete solidification time reduces by 22.87%.

ACKNOWLEDGEMENT

The authors would like to acknowledge the support of the National Natural Science Foundation of China (Grant No. 52179094).

REFERENCE

[1] Hongyi Gao, Jingjing Wang, Xiao Chen, et al., Nanoconfinement effects on thermal properties of nanoporous shapestabilized composite PCMs: A review, Nano Energy, 53 (2018) 769-797.

[2] Ke Chen, Hayder I. Mohammed, Jasim M. Mahdi, et al., Effects of non-uniform fin arrangement and size on the thermal response of a vertical latent heat triple-tube heat exchanger, Journal of Energy Storage, 45 (2022) 103723.

[3] Chenzhen Ji, ZhenQin, Swapnil Dubey, et al., Simulation on PCM melting enhancement with double-fin length arrangements in a rectangular enclosure induced by natural convection, International Journal of Heat and Mass Transfer, 127 (2018) 255-265.

[4] Murat M. Kenisarin, Khamid Mahkamov, Sol Carolina Costa, et al., Melting and solidification of PCMs inside a spherical capsule: A critical review, Journal of Energy Storage, 27 (2020) 101082.

[5] Martin Longeon, Adèle Soupart, Jean-François Fourmigué, et al., Experimental and numerical study of annular PCM storage in the presence of natural convection, Applied Energy, 112 (2013) 175-184.

[6] Hongyang Li, Chengzhi Hu, Yichuan He, et al., Effect of perforated fins on the heat-transfer performance of vertical shell-and-tube latent heat energy storage unit, Journal of Energy Storage, 39 (2021) 102647.

[7] Bohui Lu, Yongxue Zhang, Jinya Zhang, et al., Preparation, optimization and thermal characterization of paraffin/nano-Fe3O4 composite phase change material for solar thermal energy storage, Journal of Energy Storage, 46 (2022) 103928.

[8] Xiaohu Yang, Pan Wei, Xinyi Wang, et al., Gradient design of pore parameters on the melting process in a thermal energy storage unit filled with open-cell metal foam, Applied Energy, 268 (2020) 115019.

[9] Bohui Lu, Yongxue Zhang, Jianjun Zhu, et al., Enhancement of the charging and discharging performance of a vertical latent heat thermal energy

storage unit via conical shell design, International Journal of Heat and Mass Transfer, 185 (2022) 122393.
[10] Saeid Seddegh, S. Saeed Mostafavi Tehrani, Xiaolin Wang, et al., Comparison of heat transfer between cylindrical and conical vertical shell-and-tube latent heat thermal energy storage systems, Applied Thermal Engineering, 130 (2018) 1349-1362.
[11] Xiaohu Yang, Junfei Guo, Bo Yang, et al., Design of non-uniformly distributed annular fins for a shell-and-tube thermal energy storage unit, Applied Energy, 279 (2020) 115772.
[12] Saeid Seddegh, Xiaolin Wang, Mahmood Mastani Joybari, et al., Investigation of the effect of geometric and operating parameters on thermal behavior of vertical shell-and-tube latent heat energy storage systems, Energy, 137 (2017) 69-82.
[13] F. Fornarelli, S.M. Camporeale, B. Fortunato i, et al., Simplified theoretical model to predict the melting time of a shell-and-tube LHTES, Applied Thermal Engineering, 153 (2019) 51-57.
[14] Xiaohu Yang, Xinyi Wang, Zhan Liu, et al., Effect of fin number on the melting phase change in a horizontal finned shell-and-tube thermal energy storage unit, Solar Energy Materials and Solar Cells, 236 (2022) 111527.